

# Stable Li Metal Anode Enabled by Space Confinement and Uniform Curvature through Lithiophilic Nanotube Arrays


Karnpiwat Tantratian, Daxian Cao, Ahmed Abdelaziz, Xiao Sun, Jinzhi Sheng, Avi Natan, Lei Chen,\* and Hongli Zhu\*

The application of lithium (Li) metal anodes in rechargeable batteries is primarily restricted by Li dendrite growth on the metal's surface, which leads to shortened cycle life and safety concerns. Herein, well-spaced nanotubes with ultrauniform surface curvature are introduced as a Li metal anode structure. The ultrauniform nanotubular surface generates uniform local electric fields that evenly attract Li-ions to the surface, thereby inducing even current density distribution. Moreover, the well-defined nanotube spacing offers Li diffusion pathways to the electroactive areas as well as the confined spaces to host deposited Li. These structural attributes create a unique electrodeposition manner; i.e., Li metal homogeneously deposits on the nanotubular wall, causing each Li nanotube to grow in circumference without obvious sign of dendritic formation. Thus, the full-cell battery with the spaced Li nanotubes exhibits a high specific capacity of 132 mA h g<sup>-1</sup> at 1 C and an excellent coulombic efficiency of ≈99.85% over 400 cycles.

Lithium (Li) metal anode attracts enormous interests nowadays as an ideal electrode for rechargeable batteries due to its high specific capacity (3860 mA h g<sup>-1</sup>), low electrochemical potential (−3.04 V vs standard hydrogen electrode), and its low density (0.53 g cm<sup>-3</sup>).<sup>[1–3]</sup> These properties are what make Li metal batteries a promising replacement for traditional Li-ion batteries. Li-ion technology suffers from limited gravimetric energy density (<250 Wh kg<sup>-1</sup>),<sup>[4]</sup> which impedes their implementation over a wide spectrum of high-energy applications. Li metal anodes, however, still possess critical challenges that restrict its commercialization as a reliable electrode material. One of the main drawbacks is Li dendrite growth, which leads to the decay of coulombic efficiency, poor cycling performance, and even internal short circuits.<sup>[5,6]</sup>

K. Tantratian, Prof. L. Chen  
Department of Mechanical Engineering  
University of Michigan-Dearborn  
Dearborn, MI 48128-1491, USA  
E-mail: leichn@umich.edu

D. Cao, A. Abdelaziz, X. Sun, Dr. J. Sheng, A. Natan, Prof. H. Zhu  
Department of Mechanical and Industrial Engineering  
Northeastern University  
Boston, MA 02115, USA  
E-mail: h.zhu@neu.edu

 The ORCID identification number(s) for the author(s) of this article can be found under <https://doi.org/10.1002/aenm.201902819>.

DOI: 10.1002/aenm.201902819

To date, several studies show that the growth of Li dendrite starts with small nuclei, which result from either (i) the nonuniformity of the metal surface or (ii) the instability of the solid electrolyte interface (SEI) due to the large volume change.<sup>[7–9]</sup> Due to the accumulation of electric charges on the nucleation tips, the local electric field strength is very strong at these points, and attracts the large concentrations of Li-ions in the electrolyte to its sharp surface. Consequently, Li-ions are not evenly distributed, resulting in nonuniform local current density distribution at the electrode surface. Li rapidly grows on the sharp tips of the nuclei where the local current density is concentrated, while Li slowly deposits on the base where the local current density is relatively small,<sup>[7,10–12]</sup> causing Li dendrite formation as shown in

**Figure 1a.** To resolve the root causes of this problem, the ideal anode structure must feature uniform surface curvature to equalize the electric field and must be able to accommodate large volume variation during cycling as well.

Previous efforts have been made to tackle Li dendrite growth, including stabilizing the SEI layer through adding additives to the electrolytes,<sup>[13,14]</sup> increasing the electrolyte salt's concentration,<sup>[13,15]</sup> and designing an artificial layer at the electrode/electrolyte interface for dendrite suppression.<sup>[16,17]</sup> Recently, hosting Li metal inside a 3D scaffold has been found to be one of the most effective approaches to solve this challenge.<sup>[18–20]</sup> A high specific surface area of the 3D scaffold decreases the effective current density and thus delays the Li dendrite formation, in accordance with Sand's formula.<sup>[21]</sup> In addition, the 3D structure provides confined space to accommodate Li plating, mitigating massive volume changes. This strategy allows not only the utilization of different materials, but different morphologies as a host structure for Li metal, e.g., cellulose nanofibers,<sup>[22]</sup> carbon felt,<sup>[23]</sup> nickel foam,<sup>[24,25]</sup> layered reduced graphene oxide,<sup>[26]</sup> and copper nanowires.<sup>[27]</sup> Recently, vertically aligned structures, such as carbonized wood,<sup>[28]</sup> copper microchannels,<sup>[29]</sup> and nanochannels on stainless steel,<sup>[30]</sup> have gained interest because these vertically oriented structures efficiently promote Li-ion transport to the electroactive areas during plating, enhancing charge transfer kinetics. However, at higher current densities, the electrode architecture plays a bigger role in the morphological evolution of Li deposition. An excessive buildup of Li plating occurs on a sharp curvature area, introducing “hot

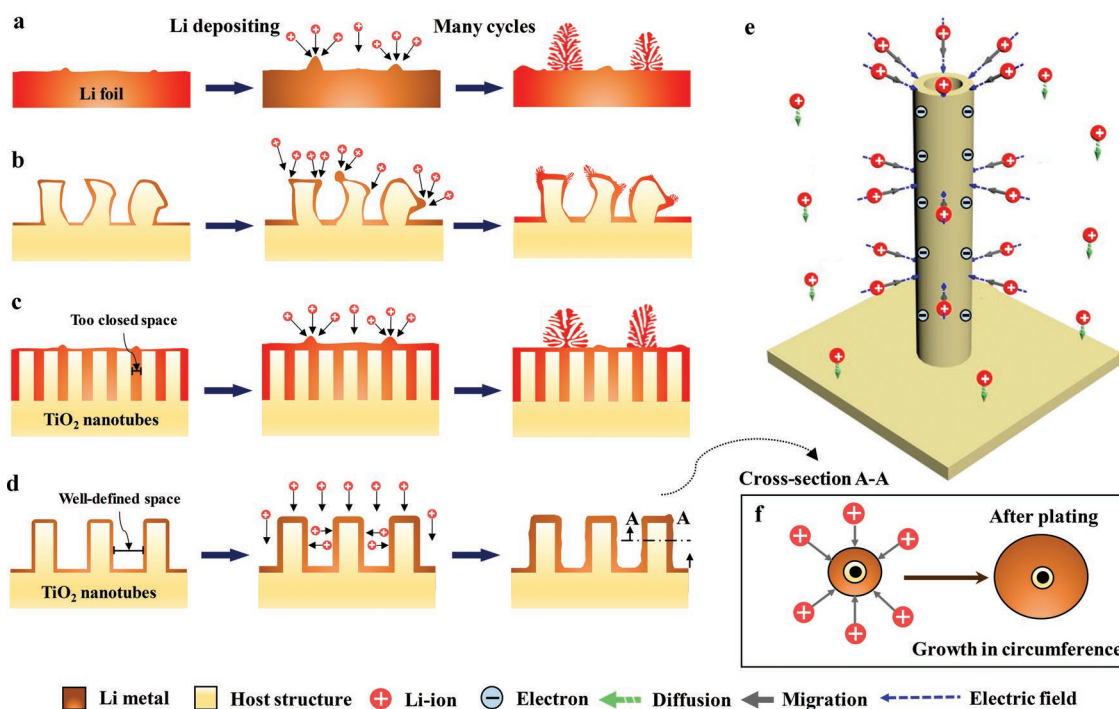


**Figure 1.** Schematic of Li deposition on four different anode structures. Li deposition on a) Li foil, b) vertically aligned structure with nonuniform surface curvature, c) closed Li nanotubes, and d) spaced Li nanotubes. e) 3D schematic illustration of Li-ion transport under the influence of diffusion and the uniform electrostatic forces that guide Li-ions to distribute over the nanotube surface uniformly. f) 2D cross-section of a Li nanotube illustrating the unique electrodeposition manner, i.e., the circumferential growth of the spaced Li nanotubes.

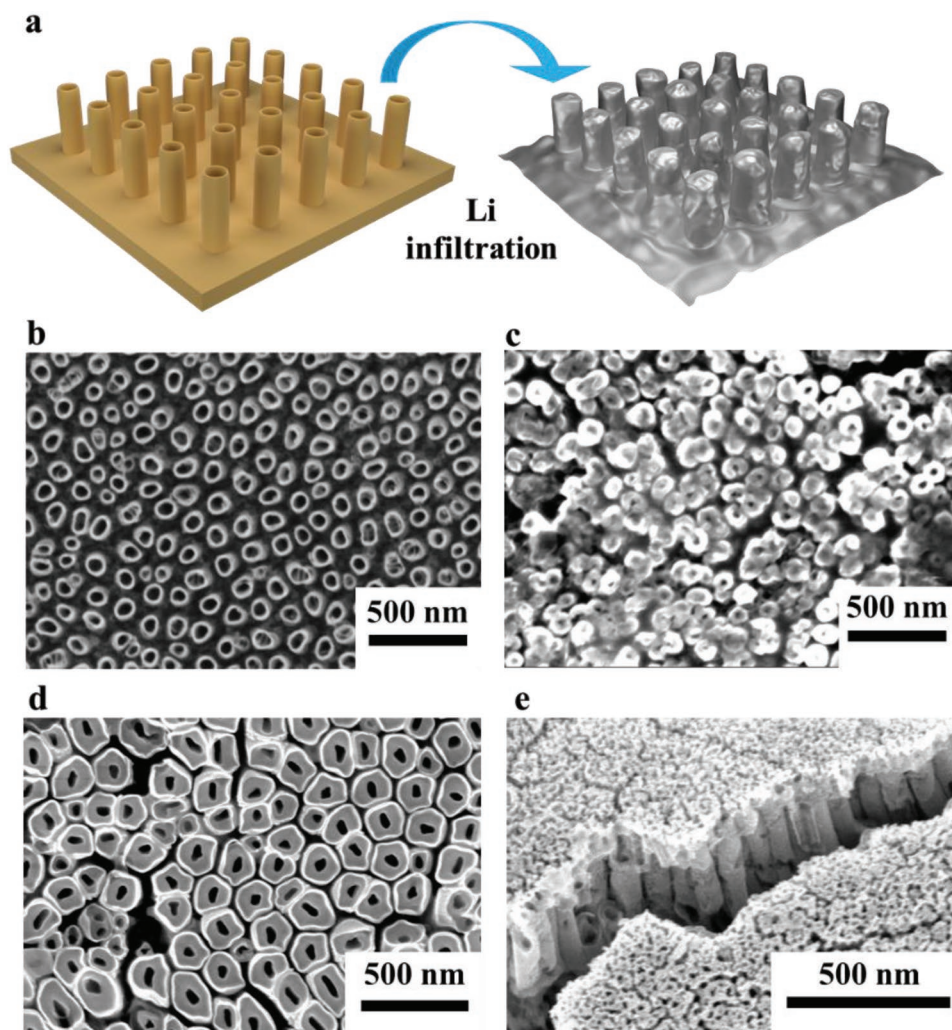
spots" for Li dendrite formation (Figure 1b).<sup>[31]</sup> Therefore, there is a strong need to develop a 3D scaffold that features uniform surface curvature along with a vertically aligned structure.

The electrochemical anodization method is well known for its capability to produce vertically oriented metal oxide nanotubular structures, such as titanium dioxide (TiO<sub>2</sub>) nanotubes.<sup>[32]</sup> By this fabrication process, vertically aligned TiO<sub>2</sub> nanotubes own uniform surface curvature. Also, TiO<sub>2</sub> nanotubes itself exhibit excellent elastic modulus (23–44 GPa),<sup>[33]</sup> indicating an ability to resist deformation under mechanical stress induced by the volume change of Li metal during cycling. Furthermore, TiO<sub>2</sub> is highly lithiophilic, so the uniform coverage of Li metal over TiO<sub>2</sub> surface is easily achieved through Li infiltration. These suggest that TiO<sub>2</sub> nanotubes may be a promising 3D scaffold for Li metal anodes. Nevertheless, self-ordered TiO<sub>2</sub> nanotube arrays are generally closely packed,<sup>[32,34]</sup> featuring little to no space between nanotubes to host Li plating. When closed nanotube arrays are used as a host structure, Li mostly grows toward the separator from the top surface of the nanotubes, eventually causing the Li dendrite problem as shown in Figure 1c. Therefore, the nanotube spacing must be widened to effectively accommodate Li plating.

In this study, we report, for the first time, vertically well-spaced TiO<sub>2</sub> nanotube arrays with ultrauniform curvature as a host structure for Li metal anode. The TiO<sub>2</sub> nanotube arrays, fabricated using a modified electrochemical anodization, exhibit uniform surface curvature, regular nanotube spacing, and vertical alignment. Molten Li metal is successfully infiltrated into the spaced TiO<sub>2</sub> nanotubes scaffold to form the spaced Li nanotubes structure, which can effectively suppress the dendrite formation as illustrated in Figure 1d. In the electrolyte solution,

Li ions move under the influences of electrostatic forces (migration) and concentration gradients (diffusion). Figure 1e shows how the electric field is distributed equally on the nanotubular wall due to the uniform surface curvature. Consequently, nearby Li-ions evenly migrate to the nanotubular surface, leading to uniform local current density distribution. Moreover, the spacing between each vertically aligned nanotube gives direct pathways that promote Li-ion diffusion to the electroactive areas and also provides confined spaces to accommodate Li growth. These electrode structural properties endow the uniform Li deposition on the nanotubular wall, resulting in the circumferential growth of Li nanotubes during plating (Figure 1f). Additionally, the underlying mechanism of this unique Li growth manner is further explained via current density distribution and phase-field models. We believe the concept of uniform surface curvature along with space confinement can be applied to develop a Li metal anode architecture that enables dendrite-free Li deposition.

The TiO<sub>2</sub> nanotube arrays with ultrauniform tubular curvature are fabricated by utilizing an electrochemical anodization technique, which is characterized by its simplicity, cost-effectiveness, and wide implementation on large-scale production.<sup>[32,34]</sup> Utilizing the conventional method, the classic closed TiO<sub>2</sub> nanotubes are obtained. But, to fabricate the spaced TiO<sub>2</sub> nanotubes, the anodization parameters such as anodization time, applied voltage, and electrolyte solution are adjusted to widen the internanotube space. Then, molten Li metal (at 450 °C) is infiltrated into the TiO<sub>2</sub> nanotubes scaffold to form the composite anode structure, called spaced Li nanotubes, as illustrated in Figure 2a. Note that due to the high lithiophilicity of TiO<sub>2</sub>, presurface treatment is not required prior to Li infiltration.



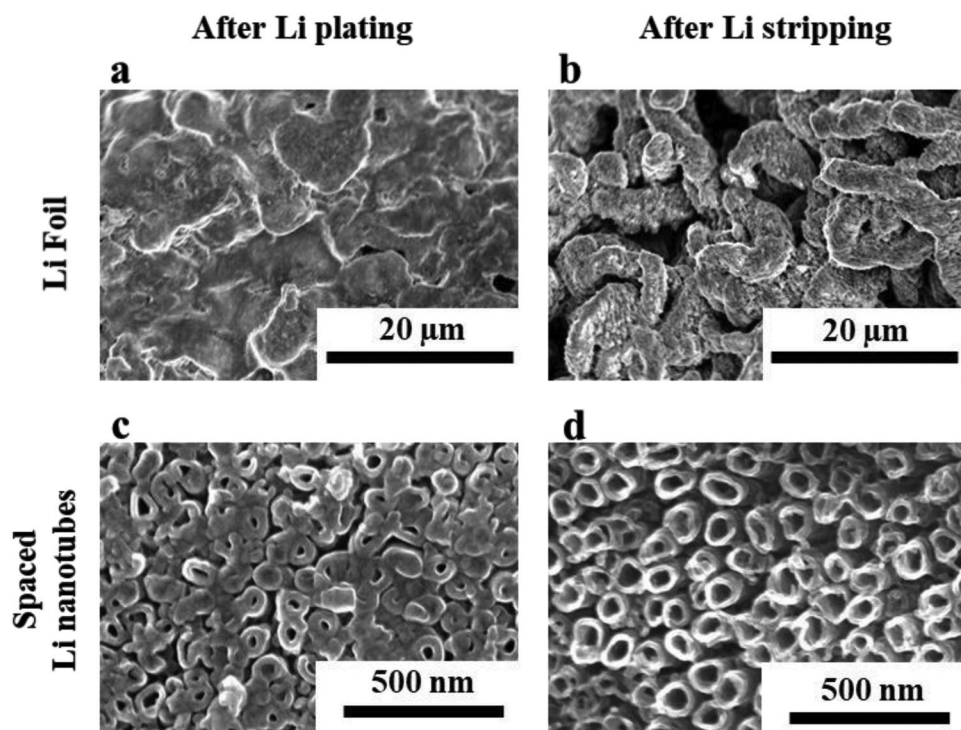
**Figure 2.** Morphological comparison between the spaced  $\text{TiO}_2$  nanotubes and the closed  $\text{TiO}_2$  nanotubes before and after Li infiltration. a) Schematic of Li infiltration into the  $\text{TiO}_2$  anodized nanotubes. Scanning electron microscopy (SEM) top-view images of the spaced  $\text{TiO}_2$  nanotubes b) before and c) after Li infiltration. SEM top-view and tilted view images of the closed  $\text{TiO}_2$  nanotubes d) before and e) after Li infiltration.

Figure 2b shows the scanning electron microscopy (SEM) image of the spaced  $\text{TiO}_2$  nanotube scaffold before Li infiltration. Obviously, the structure is composed of vertically oriented nanotubes with  $70 \pm 20$  nm diameter,  $125 \pm 50$  nm internanotube space, and uniform surface curvature. The thickness of the  $\text{TiO}_2$  nanotubes is around 15–20 nm. During Li infiltration, molten Li metal uniformly spreads over the  $\text{TiO}_2$  nanotubes surface due to (i) its low viscosity at  $450^\circ\text{C}$  and (ii) the excellent lithiophilic surface of  $\text{TiO}_2$  that allows molten Li to flow into the structure under capillary action. After Li infiltration, Figure 2c shows the uniform coverage of Li metal over the  $\text{TiO}_2$  nanotubes surface. Furthermore, the resulting Li nanotube arrays still possess the moderate spacing between nanotubes, which allows for host Li metal growth and improves ionic transport with its vertical carrier pathway. For comparison, we also measured the closed  $\text{TiO}_2$  nanotube arrays. Figure 2d displays little to very narrow nanotube spacing. After Li infiltration, Li metal barely infuses into the nanotubular structure, but instead mostly covers the top surface and occasionally closes pores as illustrated in Figure 2e. The lighter contrast observed on the nanotubes is Li, which is

highly sensitive to the electron beam. The  $\text{TiO}_2$  has low electrical conductivity. However, the Li metal layer covering the entire  $\text{TiO}_2$  nanotube surface is electrically conductive. Thus, Li deposits on the uniform surface of the Li metal layer during Li plating, not directly on the  $\text{TiO}_2$  surface. Therefore, the poor coverage of Li metal could result in a decrease in the electroactive area and an absence of the confined spaces.

To explore the surface morphology after cycling, SEM images of the spaced Li nanotubes and the Li foil counterparts were taken after 100 cycles at current density of  $1\text{ mA cm}^{-2}$ . The pristine Li foil itself has an irregular bare surface (Figure S1, Supporting Information). The roughness of the metal surface overwhelmingly contributes to the inhomogeneous distribution of local current density on the electrode/electrolyte interface. As a result, the nonuniform Li deposition on the Li foil surface is observed, as shown in Figure 3a. At the stripping state, the severe Li dendrite formation is evident in Figure 3b. On the contrary, the spaced Li nanotubes exhibit uniform tubular curvature (Figure 2c) that induces even current density distribution throughout its surface. After Li plating, the thickness of each





**Figure 3.** Morphological evolution of Li deposition. SEM images of Li foil surface a) after Li plating and b) after Li stripping at the 100th cycle. SEM images of the spaced Li nanotubes surface c) after Li plating and d) after Li stripping at the 100th cycle.

Li nanotube is increased to 30–35 nm without any sign of Li dendrite formation (Figure 3c). The newly deposited Li consistently forms a uniform layer covering the previously deposited Li on the nanotubular wall. Consequently, the thickness of each Li nanotube continuously increases with time, showing a very unique electrodeposition behavior. In addition, the Li growth direction is parallel to the separator, and the deposited Li remains confined in the internanotube space. Figure 3d shows the thickness of spaced Li nanotubes is reduced to 16–21 nm after Li stripping. Due to an excellent mechanical and chemical strength of  $\text{TiO}_2$  nanotube arrays, the nanotubular morphology with uniform curvature is still stable after 100 cycles, indicating the robustness of the scaffold. Furthermore, the Li deposition morphology on the closed Li nanotubes after cycling is also investigated. As observed from Figure S2 (Supporting Information), Li metal barely resides in the nanotube spacing, but deposits on the top surface of the nanotubes, forming a moss-like Li dendrite. Clearly, the nanotubes with the closed tube spacing could not suppress the Li dendrite formation due to the lack of space confinement.

To further explain the difference between the Li deposition mechanisms for the spaced Li nanotubes, compared to the closed Li nanotubes and Li foil, a nonlinear phase-field model with mass transport and charge conservation equations analysis was performed to simulate the Li deposition. The size of the electrolyte domain for all anode structures is  $1.2 \times 1.2 \mu\text{m}$ . For the spaced Li nanotubes, diameter, length, and tube spacing are 90 nm, 650 nm, and 150 nm, respectively, while for the closed Li nanotubes, the tube spacing is 50 nm. The Li deposition behaviors were simulated under the overpotential of 0.1 V. On the Li foil surface, small Li nucleation sites occur at the electrode/electrolyte interface during cycling primarily due to the nonuniformity of

the electrode surface. The tips of the nucleation sites induce the large Li-ion concentration,<sup>[12]</sup> leading to the increase of local current density. Li grows rigorously on the tips, thus resulting in the growth of Li dendrites as observed in Figure 4a. Figure 4b illustrates that Li-ions are distributed unevenly, corresponding to the dendritic shape. Figure 4c displays that the current density is concentrated only at the dendrite tips. On the contrary, Figure 4d shows the uniform Li deposition on the spaced Li nanotubes. In Figure 4e, Li-ions are distributed uniformly over the nanotubular surfaces. The spacing between vertically aligned nanotubes guides Li-ions moving vertically downward into the electroactive surface area. So, the ample amounts of Li-ions, which are ready for further Li deposition on the nanotubular wall, are present in the nanotube spacing. In Figure 4f, the current density distribution is homogeneous throughout the nanotubular walls due to uniform surface curvature. As a result, Li metal continues growing uniformly on the nanotube surface and is confined in the internanotube spaces. However, for the closed Li nanotubes, Li deposition mostly happens at the top of the nanotubes, causing a wavy-like surface as shown in Figure 4g. Figure 4h shows Li-ions are concentrated near the top of the nanotubes. The current density profile follows the irregular surface of the deposited Li metal (Figure 4i). These findings imply that further Li deposition would occur on the irregular surface in the direction of the separator without space confinement. The wavy surface of deposited Li together with the accumulation of current density makes the electrode/electrolyte interface susceptible to the Li nucleation sites that eventually cause Li dendrite growth. Note that the primary purpose of this modeling is to illustrate the electrochemical behaviors for the three cases. Several assumptions (e.g., without the SEI layer and Li plating/stripping

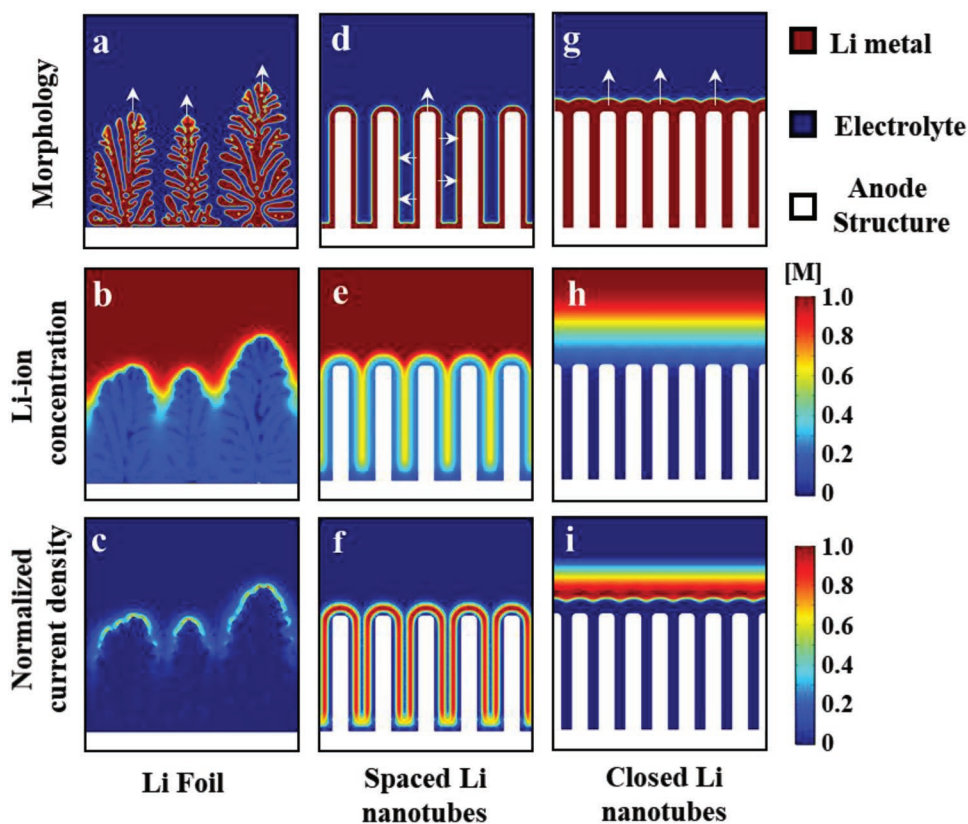


**Figure 4.** The simulated Li deposition morphology on a) Li foil, d) the spaced Li nanotubes, and g) the closed Li nanotubes at a simulation time of 800 s with the size of domain as  $1.2 \times 1.2 \mu\text{m}$  (white arrows indicate the Li growth directions). The Li-ion concentration distribution in the electrolyte near b) Li foil, e) the spaced Li nanotubes, and h) the closed Li nanotubes. The normalized local current density profile for c) Li foil, f) the spaced Li nanotubes, and i) the closed Li nanotubes.

cycling involved) were made to make the model mathematically tractable, and the improvement of the model for quantitative investigations on Li deposition is still underway.

According to the characteristic of a conducting object, the area of the highest curvature develops the greatest electric field strength out of its surface. In the electrodeposition system, blunt points, edges, and sharply curved areas on the electrode surface produce the most intense local electric fields. This electric field attracts a huge amount of surrounding Li-ions to the sharp points, leading to the inhomogeneous distribution of local current density, and consequently Li dendrite growth. On the contrary, the electric field strength on the electrode surface is homogeneous at the locations where the surface curvature is uniform. Li-ions evenly migrate to the electrode surface, leading to the uniform distribution of local current density, which contributes to the uniform Li deposition. Within, the current density distribution modeling was performed to understand the underlying mechanism of ionic diffusion and migration near the Li nanotubes surface.

**Figure 5a** shows the current density is distributed uniformly over the nanotubular walls, which is attributed to the ultrauniform nanotube structure. Moreover, **Figure 5b,c** illustrates that at the simulation time,  $t_0 = 5 \text{ ms}$  (the time at which the system reaches steady state), the current density and Li-ion concentration distribution in the electrolyte are homogeneously accumulated near the nanotubular wall. On the contrary, with a nonuniform tubular shape, the current density distribution is nonuniform

over the nanotubular wall due to the inhomogeneous Li-ion concentration at the surface (**Figure 5d**). The current density and Li-ion concentration distribution near the nanotube surface are not as homogenous as the uniform sample (**Figure 5e,f**). In this case, as evident from **Figure 5g**, the concave curve in the middle of the nonuniform nanotube contributes to uneven current density distribution. **Figure 5h** shows that along the outer surface of the nanotube (at  $z = 325 \text{ nm}$ ), the current density is relatively high at the more curved areas, while the ultrauniform nanotubular structure exhibits a flat current density profile.

Nevertheless, sharp edges are inevitable in any tube structure, leading to the highest local current density. However, this problem is insignificant in the case of the nano-sized structure because the difference in a degree of curvature between the nanotube body and its edge is insignificant. To elaborate on this theory, we investigated the preference of the nanotubular electrodes compared to the microtubular electrodes. The dimensions of the microtube used herein are ten times larger than the ultrauniform nanotube. The normalized current density along the tube length for the uniform nanotube and microtube at the steady state is plotted in **Figure S3a** (Supporting Information). The difference in magnitude of local current density between the tube body and its edge is clearly observed for the microtube, while the current density along the length of the nanotube is almost uniform. In addition, at the time  $t_0$  (the time at which Li-ions evenly distribute on the nanotube surface), Li-ions are

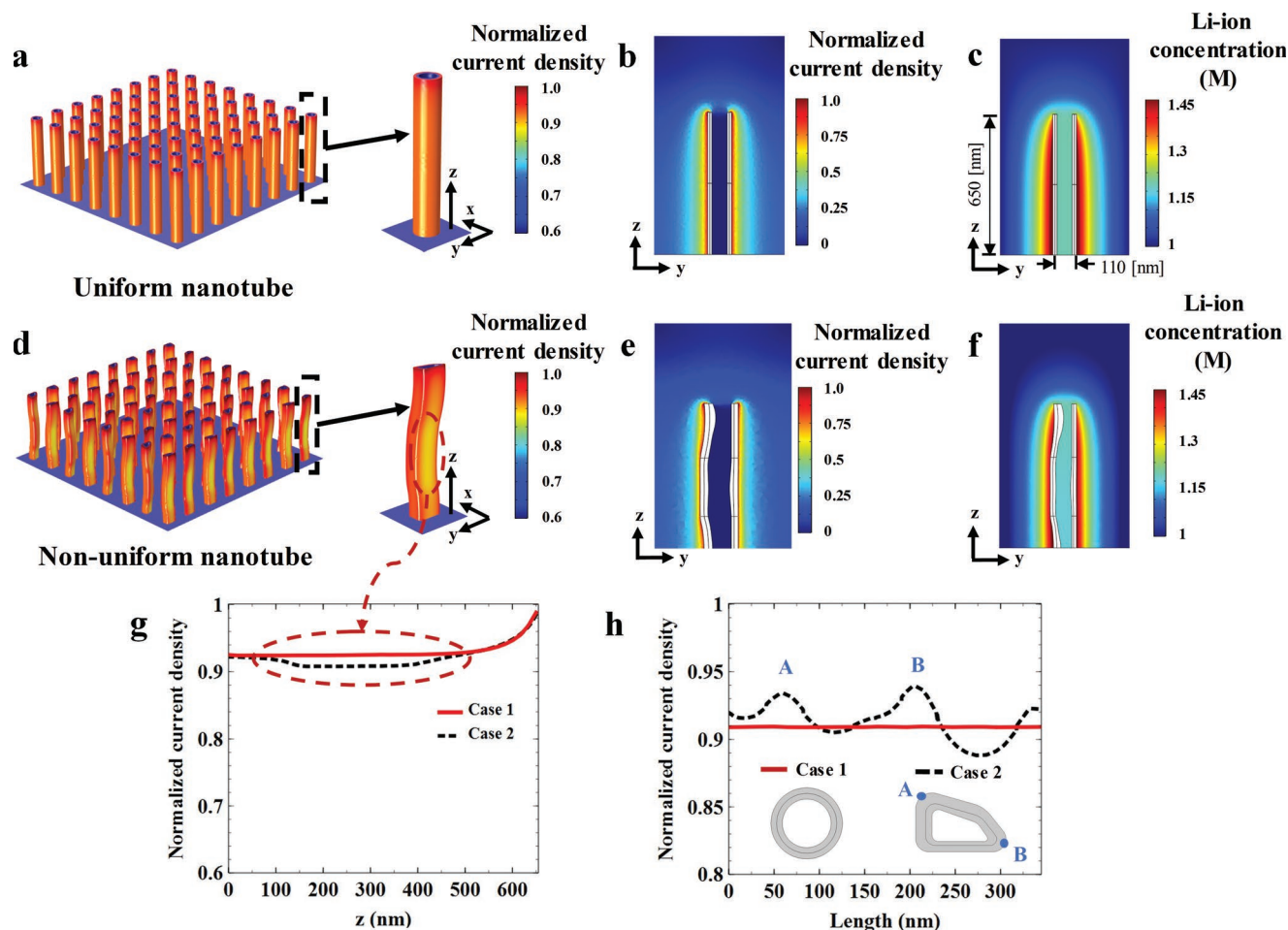


**Figure 5.** Simulation results for current density distribution modeling. a) The current density distribution over the Li nanotubes surfaces with ultrauniform curvature. 2D plots of b) the normalized current density and c) Li-ion concentration distributions in the electrolytes near the ultrauniform nanotube wall at the simulation time,  $t_0 = 5$  ms (the time at which the system reaches steady state). d) The current density distribution over the Li nanotubes surfaces with nonuniform morphology. 2D plots of e) the normalized current density and f) Li-ion concentration distributions in the electrolytes near the nonuniform morphology at the simulation time,  $t_0$ . g) A comparison plot of current density distribution on the nanotubes surface along the  $z$ -direction. h) A comparison plot of current density distribution along the perimeter of the nanotubes cross-section at  $z = 325$  nm.

only accumulated at the top of the microtube (Figure S3b, Supporting Information). Interestingly, Li-ions take a greater amount of time to distribute over the microtube surface uniformly (Figure S3c, Supporting Information). The longer the time it takes for Li-ions to distribute over the electrode surface equally, the higher the chance it has for nonuniform Li deposition. Therefore, an excessive buildup of Li deposition is more likely to occur on the edges of the microtubes than on the nanotubes.

In order to assess the stability of Li metal electrodes, electrochemical measurements have been conducted using symmetric coin cells. The tests on three different electrode structures are performed: (i) the spaced Li nanotubes, (ii) the closed Li nanotubes, and (iii) bulky Li foils. Electrochemical cycling was performed for 225 cycles (450 h) at a current density of  $4 \text{ mA cm}^{-2}$  and a charging capacity of  $4 \text{ mA h cm}^{-2}$ . In Figure 6a, the three samples show similar stability at the first 60 cycles, though the Li foil sample shows slightly high cycling overpotential (Figure 6b). At the 70th cycle, the Li foil symmetric cell exhibits a significant increase in the overpotential with large hysteresis, which is mainly related to

the Li dendrite formation (Figure 6c). At the 150th cycle, the magnitude of overpotential for the closed Li nanotubes starts to increase as cycling number increases. At the 200th cycle, the closed Li nanotubes sample exhibits much greater overpotential (0.15 V) than the spaced Li nanotubes sample (0.05 V), indicating a decline in the stability of the closed Li nanotubes electrode (Figure 6d). The spaced Li nanotubes cell shows the highest stability over the cycling period, without any voltage hysteresis.

To study the interface stability, we investigated the interfacial resistance for these three samples using electrochemical impedance spectroscopy (EIS) measurements and then obtained the Nyquist plots for the symmetric cells. The high-frequency semicircle represents the interfacial resistance and the charge transfer resistance at the electrode/electrolyte interface. The intersection of the high-frequency semicircle with the Re ( $Z$ ) axis represents the overall ohmic resistance of the cell. Figure 6e shows the EIS obtained before cycling. The spaced Li nanotubes symmetric cell shows the lowest interfacial impedance, while the pristine Li foil sample exhibits the highest interfacial impedance. This is probably because the spaced Li nanotubes structure provides the



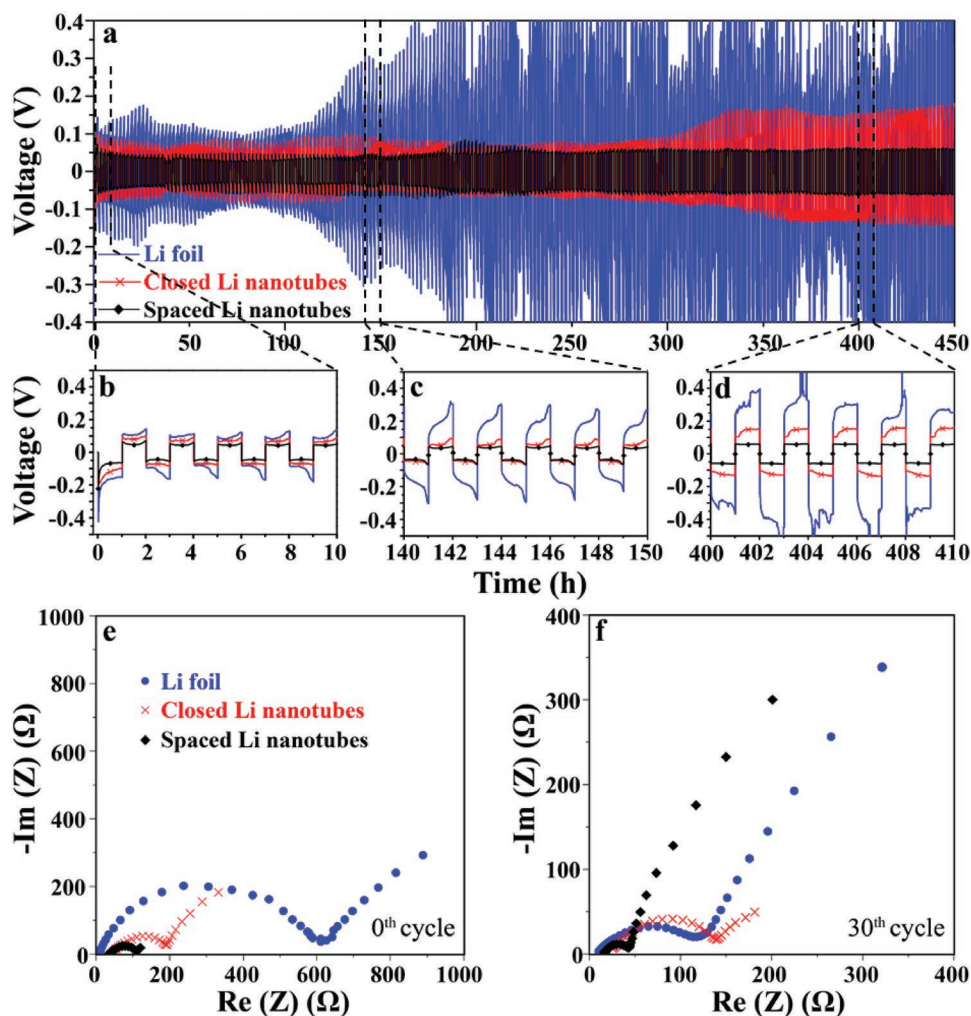


**Figure 6.** Electrochemical measurements of the symmetric cells constructed with Li foil, the closed Li nanotubes, and the spaced Li nanotubes. a) Cycling at the current density of  $4 \text{ mA cm}^{-2}$  and cycling capacity of  $4 \text{ mA h cm}^{-2}$ . Variation of the overpotential at b) 0–10 h, c) 140–150 h, and d) 400–410 h. Electrochemical impedance spectroscopy (EIS) for the three samples e) before cycling and f) after the 30th cycle.

largest electrode/electrolyte contact area, improving the charge transfer kinetics at the electrode interface. After the 30th cycle at the current density of  $4 \text{ mA cm}^{-2}$ , the interfacial resistances of the three samples are greatly reduced as a result of the oxide layer removal during cycling (Figure 6f). However, the spaced Li nanotubes cell still possesses the lowest interfacial resistance. Such a small overall resistance indicates outstanding interfacial stability and favorable charge transport at the interface. We attribute the low interfacial impedance of the spaced Li nanotubes to its structural characteristics: (i) the uniform curvature that ensures uniform current density distribution, stabilizing the electrode/electrolyte interface, and (ii) the nanotube spacing that provides diffusion pathways for Li-ions to spread over the electroactive surface, enhancing charge transfer kinetics.

Moreover, to further study the influence of the surface curvature on the electrochemical performances, a controlled experiment was carried out. The Li infiltration method is used to obtain a Li metal anode composited on a wood-based scaffold with random surface curvature (Figure S4a, Supporting Information). After the 100th cycle, under  $4 \text{ mA cm}^{-2}$  current density

and  $4 \text{ mA h cm}^{-2}$  cycling capacity, Figure S4b (Supporting Information) shows a huge change in the electrode morphology. The inhomogeneous Li plating is evident, which impedes electrochemical performance. Thus, the cycling stability of the symmetric cell shows a large overpotential only after the 15th cycle (Figure S4c, Supporting Information), indicating the poor interfacial stability of the wood-based electrode.

The spaced Li nanotubes and its Li foil counterpart are used as the anodes in two different cells, with  $\text{LiFePO}_4$  used as the cathode for both cells. As shown in Figure 7a, the cell with the spaced Li nanotubes reveals excellent specific capacity even under the high charging rate ( $85 \text{ mA h g}^{-1}$  at 10 C), which significantly surpasses its Li foil electrode counterpart ( $10 \text{ mA h g}^{-1}$  at 10 C). The cell stability is further investigated using current rate at 1 C. The cell with the spaced Li nanotubes shows great robustness with a coulombic efficiency of  $\approx 99.85\%$  over 400 cycles (Figure 7b). No significant decay is observed over cycling with an average specific capacity of  $132 \text{ mA h g}^{-1}$ . On the other hand, with the Li foil anode, the specific capacity of the cell decays continuously during cycling from  $120 \text{ mA h g}^{-1}$

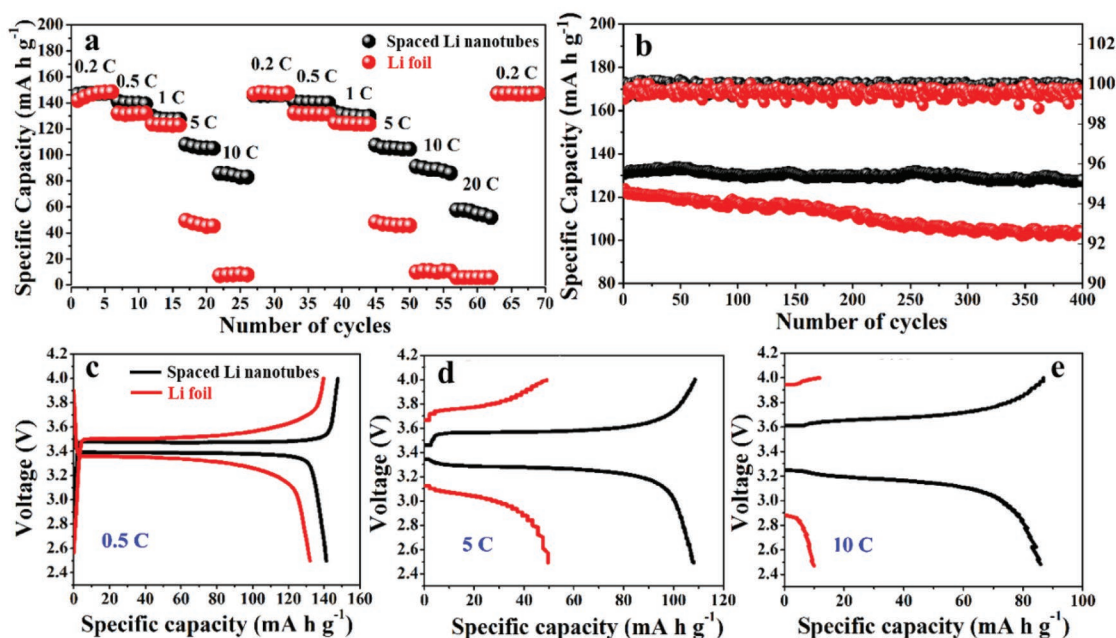


**Figure 7.** Electrochemical performance of full-cell batteries with LiFePO<sub>4</sub>/the spaced Li nanotubes and LiFePO<sub>4</sub>/Li foil. a) Rate capability at various rates from 0.2 to 20 C. b) Coulombic efficiency calculated at 1 C. Voltage profile comparison for each cell at c) 2 C, d) 5 C, and e) 10 C.

to 95 mA h g<sup>-1</sup>. The voltage profiles for both cells at 0.5, 5, and 10 C are shown in Figure 7c–e, respectively. As observed, the cell with the spaced Li nanotubes shows a flatter voltage plateau at 0.5 C with a lower overpotential for both the charging and discharging cycles, compared to the cell comprised of Li foil anode. At 5 and 10 C charging rates, the overpotential for the cell with Li foil significantly increases, while the cell with the spaced Li nanotubes still shows a flat voltage plateau, indicating better rate performance. The large specific capacity and exceptional coulombic efficiency at the high charging rate for the cell with the spaced Li nanotubes are of great importance in high-energy applications that require fast charging/discharging speed with reliable performance and long-term stability.

We investigated an effective solution to address the Li dendrite problem by introducing uniform and spaced Li nanotubes array as Li metal anode architecture. The spaced Li nanotubes are constructed by infiltrating molten Li metal into a well-spaced TiO<sub>2</sub> nanotubes scaffold. The spaced Li nanotubes anode possesses two crucial structural characteristics that effectively address the causes of Li dendrite growth: (i) ultrauniform surface curvature and (ii) well-defined nanotube spacing. First, ultrauniform surface curvature homogenizes the local current density at the nanotube wall. This fundamental mechanism has been proved through current density distribution modeling. The homogenized current density leads to the uniform Li growth on the nanotube surface. Also, such a uniform Li deposition behavior is considerably less likely to cause the mechanical rupture of the SEI layer, contributing to high interfacial stability during cycling. This approach to suppress Li dendrite growth is applicable to all types of electrolytes and remains effective if uniform surface curvature of the electrode is present. Second, the well-defined nanotube spacing not only provides direct Li-ion diffusion pathways but also confined spaces. The spacing between vertically aligned Li nanotubes guides Li-ions moving directly into the electroactive

area, improving the charge transfer kinetics at the electrode interface. Moreover, the sufficient space between nanotubes could host the uniform Li deposition on the nanotubular wall, allowing each Li nanotube to steadily grow in circumference during Li plating. In addition, Li deposition direction is parallel to the separator instead of perpendicular to the separator, which helps to alleviate safety concerns. Furthermore, the nanotube spacing impacts the cell stability and performance. Within this research, we demonstrate that, when compared to the spaced Li nanotubes, the closed Li nanotubes less effectively suppress Li dendrite growth, show lower interfacial stability, and have inferior cycling stability. Nevertheless, the effects of different nanotube spacing on the Li deposition morphology and cell performance have not yet been thoroughly investigated. To find an optimum design for the nanotube spacing, more efforts are needed.

In summary, this work presents spaced Li nanotube arrays with ultrauniform curvature as a Li metal anode structure. Due to the metal oxide's uniform tubular curvature and its well-defined nanotube spacing, Li uniformly deposits on the nanotubular wall, causing individual Li nanotubes to get thicker over time during Li plating. Thus, the full-cell battery with LiFePO<sub>4</sub> cathode and spaced Li nanotubes anode shows an excellent specific capacity of 132 mA h g<sup>-1</sup> under high charging rate (1 C), with a coulombic efficiency of ≈99.85% over 400 cycles. We believe the uniform curvature of the anode structure, as well as the space confinement, is the key to achieving these highly stable Li metal anodes. This novel nanotubular electrode architecture takes an inspiring step toward improving the reliability of Li metal anode.

## Experimental Section

**TiO<sub>2</sub> Nanotube Preparation:** The spaced TiO<sub>2</sub> nanotube arrays were fabricated via a modified anodization process. The electrolyte used



was 0.25 wt% ammonium fluoride (NH<sub>4</sub>F) (99%, Sigma-Aldrich) in anhydrous ethylene glycol (99.8%, Sigma-Aldrich) at room temperature. Titanium (Ti) foils (Sigma-Aldrich) with a thickness of 0.25 mm were cleaned by sonicating them in acetone and ethanol consecutively. They were then rinsed with deionized (DI) water and dried in an oven. The Ti foil served as the anode with platinum as the counter electrode. To obtain the well-spaced TiO<sub>2</sub> nanotube arrays, the anodization was performed under 36 V for 1 h in the ethylene glycol solution with 1 wt% of NH<sub>4</sub>F and 4 wt% of DI water. In contrast, the TiO<sub>2</sub> nanotube arrays with narrow space were fabricated under 130 V for 1 h in the ethylene glycol solution with 0.5 wt% of NH<sub>4</sub>F.

**Li Infiltration:** The TiO<sub>2</sub> nanotube arrays were transferred into an argon-filled glove box. Lithium ribbons (99.9%, Sigma-Aldrich) were scraped using blades in order to get rid of any surface oxide layer. Afterward, Li metal was melted to 450 °C, at which TiO<sub>2</sub> nanotube arrays were put in contact with the molten surface. After molten Li infused into the nanotube structure, the composite Li/TiO<sub>2</sub> was left to be cooled to room temperature before being used as the electrode. Note that the titanium foil was little fragile and required caution. However, after lithium infiltration, the structure became very robust and easily handled.

**Electrochemical Characterizations:** For the galvanostatic symmetric cell test, two identical electrodes were assembled with (2025-MTI) coin cell type. In this setup, the three electrodes samples were Li foil, the spaced Li nanotubes, and the closed Li nanotubes. For the full-cell tests, the spaced Li nanotubes were used as the anode, whereas LiFePO<sub>4</sub> was used as the cathode. For its counterpart, Li foil was used as the anode instead, and LiFePO<sub>4</sub> was used as the cathode. The active cathode material was prepared with polyvinylidene fluoride (MTI) and carbon black with a ratio of 8:1:1 in *N*-methyl-2-pyrrolidone solvent. The electrolyte used in all of the tests was 1 M Li bis(trifluoromethanesulfonyl)imide dissolved in 1:1 v/v 1,3-dioxolane/1,2-dimethoxyethane with 2 wt% Li nitrate. Celgard 2325 (25 μm) was used as the separator. For the measurements, galvanostatic cycling tests were performed using LANDTH 8-channel tester. The electrochemical impedance spectroscopy tests were carried out using Biologic VMP3 potentiostat ranging from 1 MHz to 100 mHz, and the amplitude was 5 mV.

## Supporting Information

Supporting Information is available from the Wiley Online Library or from the author.

## Acknowledgements

K.T. and D.C. contributed equally to this work. H.Z. acknowledges the financial support from NSF CBET-1924534. H.Z. also acknowledges the Kostas Nanomanufacturing Research Center for sharing the scanning electron microscope. L.C. is thankful for the financial support by NSF-CBET-1604104.

## Conflict of Interest

The authors declare no conflict of interest.

## Keywords

electrodeposition, lithium metal anodes, phase-field simulation, TiO<sub>2</sub> nanotubes, uniform curvature

Received: August 29, 2019

Revised: October 21, 2019

Published online: November 27, 2019

- [1] H. Kim, G. Jeong, Y. U. Kim, J. H. Kim, C. M. Park, H. J. Sohn, *Chem. Soc. Rev.* **2013**, 42, 9011.
- [2] W. Xu, J. Wang, F. Ding, X. Chen, E. Nasybulin, Y. Zhang, J. G. Zhang, *Energy Environ. Sci.* **2014**, 7, 513.
- [3] A. Manthiram, Y. Fu, S.-H. Chung, C. Zu, Y.-S. Su, *Chem. Rev.* **2014**, 114, 11751.
- [4] A. Manthiram, *ACS Cent. Sci.* **2017**, 3, 1063.
- [5] M. Armand, J.-M. Tarascon, *Nature* **2008**, 451, 652.
- [6] T. Ohzuku, *J. Electrochem. Soc.* **1993**, 140, 2490.
- [7] L. Li, S. Li, Y. Lu, *Chem. Commun.* **2018**, 54, 6648.
- [8] K. Nishikawa, T. Mori, T. Nishida, Y. Fukunaka, M. Rosso, T. Homma, *J. Electrochem. Soc.* **2010**, 157, A1212.
- [9] M. D. Tikekar, L. A. Archer, D. L. Koch, *Sci. Adv.* **2016**, 2, e1600320.
- [10] C. Brissot, M. Rosso, J. N. Chazalviel, S. Lascaud, *J. Power Sources* **1999**, 81–82, 925.
- [11] P. Bai, J. Li, F. R. Brushett, M. Z. Bazant, *Energy Environ. Sci.* **2016**, 9, 3221.
- [12] L. Chen, H. W. Zhang, L. Y. Liang, Z. Liu, Y. Qi, P. Lu, J. Chen, L. Q. Chen, *J. Power Sources* **2015**, 300, 376.
- [13] J. Qian, W. A. Henderson, W. Xu, P. Bhattacharya, M. Engelhard, O. Borodin, J. G. Zhang, *Nat. Commun.* **2015**, 6, 6362.
- [14] X. Q. Zhang, X. B. Cheng, X. Chen, C. Yan, Q. Zhang, *Adv. Funct. Mater.* **2017**, 27, 1605989.
- [15] L. Suo, Y. S. Hu, H. Li, M. Armand, L. Chen, *Nat. Commun.* **2013**, 4, 1481.
- [16] H. Zhang, X. Liao, Y. Guan, Y. Xiang, M. Li, W. Zhang, X. Zhu, H. Ming, L. Lu, J. Qiu, Y. Huang, G. Cao, Y. Yang, L. Mai, Y. Zhao, H. Zhang, *Nat. Commun.* **2018**, 9, 1.
- [17] Q. C. Liu, J. J. Xu, S. Yuan, Z. W. Chang, D. Xu, Y. Bin Yin, L. Li, H. X. Zhong, Y. S. Jiang, J. M. Yan, X. B. Zhang, *Adv. Mater.* **2015**, 27, 5241.
- [18] Z. Liang, D. Lin, J. Zhao, Z. Lu, Y. Liu, C. Liu, Y. Lu, H. Wang, K. Yan, X. Tao, Y. Cui, *Proc. Natl. Acad. Sci. USA* **2016**, 113, 2862.
- [19] H. Ye, S. Xin, Y. X. Yin, Y. G. Guo, *Adv. Energy Mater.* **2017**, 7, 1.
- [20] A. M. Hafez, Y. Jiao, J. Shi, Y. Ma, D. Cao, Y. Liu, H. Zhu, *Adv. Mater.* **2018**, 30, 1802156.
- [21] H. J. S. Sand, *Philos. Mag.* **1901**, 1, 45.
- [22] D. Cao, Y. Xing, K. Tantratian, X. Wang, Y. Ma, A. Mukhopadhyay, Z. Cheng, Q. Zhang, Y. Jiao, L. Chen, H. Zhu, *Adv. Mater.* **2019**, 31, 1.
- [23] X. Y. Yue, X. L. Li, W. W. Wang, D. Chen, Q. Q. Qiu, Q. C. Wang, X. J. Wu, Z. W. Fu, Z. Shadike, X. Q. Yang, Y. N. Zhou, *Nano Energy* **2019**, 60, 257.
- [24] S. Sen Chi, Y. Liu, W. L. Song, L. Z. Fan, Q. Zhang, *Adv. Funct. Mater.* **2017**, 27, 1.
- [25] X. Y. Yue, W. W. Wang, Q. C. Wang, J. K. Meng, Z. Q. Zhang, X. J. Wu, X. Q. Yang, Y. N. Zhou, *Energy Storage Mater.* **2018**, 14, 335.
- [26] D. Lin, Y. Liu, Z. Liang, H. W. Lee, J. Sun, H. Wang, K. Yan, J. Xie, Y. Cui, *Nat. Nanotechnol.* **2016**, 11, 626.
- [27] L. L. Lu, J. Ge, J. N. Yang, S. M. Chen, H. Bin Yao, F. Zhou, S. H. Yu, *Nano Lett.* **2016**, 16, 4431.
- [28] Y. Zhang, W. Luo, C. Wang, Y. Li, C. Chen, J. Song, J. Dai, E. M. Hitz, S. Xu, C. Yang, Y. Wang, L. Hu, *Proc. Natl. Acad. Sci. USA* **2017**, 114, 3584.
- [29] S. H. Wang, Y. X. Yin, T. T. Zuo, W. Dong, J. Y. Li, J. L. Shi, C. H. Zhang, N. W. Li, C. J. Li, Y. G. Guo, *Adv. Mater.* **2017**, 29, 1.
- [30] W. Liu, D. Lin, A. Pei, Y. Cui, *J. Am. Chem. Soc.* **2016**, 138, 15443.
- [31] G. Yoon, S. Moon, G. Ceder, K. Kang, *Chem. Mater.* **2018**, 30, 6769.
- [32] P. Roy, S. Berger, P. Schmuki, *Angew. Chem., Int. Ed.* **2011**, 50, 2904.
- [33] T. Shokuhfar, G. K. Arumugam, P. A. Heiden, R. S. Yassar, C. Friedrich, *ACS Nano* **2009**, 3, 3098.
- [34] G. K. Mor, O. K. Varghese, M. Paulose, K. Shankar, C. A. Grimes, *Sol. Energy Mater. Sol. Cells* **2006**, 90, 2011.